

Vacuum evaporated porous silicon photonic interference filters

Kate Kaminska, Tim Brown, Gisia Beydaghyan, and Kevin Robbie

Porous materials with nanometer-scale structure are important in a wide variety of applications including electronics, photonics, biomedicine, and chemistry. Recent interest focuses on understanding and controlling the properties of these materials. Here we demonstrate porous silicon interference filters, deposited in vacuum with a technique that enables continuous variation of the refractive index between that of bulk silicon and that of the ambient ($n \sim 3.5$ to 1). Nanometer-scale oscillations in porosity were introduced with glancing angle deposition, a technique that combines oblique deposition onto a flat substrate of glass or silicon in a high vacuum with computer control of substrate tilt and rotation. Complex refractive index profiles were achieved including apodized filters, with Gaussian amplitude modulations of a sinusoidal index variation, as well as filters with index matching antireflection regions. A novel quintic antireflection coating is demonstrated where the refractive index is smoothly decreased to that of the ambient, reducing reflection over a broad range of the infrared spectrum. Optical transmission characteristics of the filters were accurately predicted with effective medium modeling coupled with a calibration performed with spectroscopic ellipsometry. © 2003 Optical Society of America

OCIS codes: 160.4670, 350.2460, 220.1230, 310.1860, 260.2130, 310.1210.

1. Introduction

Modern thin film optical coatings enable complex filter designs with sharp transitions, excellent control of out-of-band interference, and acceptable index matching.^{1,2} Rugate filter designs,³⁻⁵ where the refractive index varies sinusoidally with thickness, offer advantages over more common stepped index filters with thinner coatings, suppression of higher-order stop-band harmonics, and novel response including arbitrary index matching,⁶⁻⁸ multiple stop bands⁹ with application in high red-shift quasar detection,¹⁰ and predicted quasi-photonic crystals.¹¹ The rugate index profile produces a minus filter transmission response; the filter reflects incident radiation in a given spectral region (stop band), while allowing all other wavelengths to pass freely (passbands).¹² The stop band in minus filters is typically accompanied by undesirable sidelobes in the transmission regions, whose strength is a function of the mismatch between the index of the rugate and the surrounding media. Southwell,¹³ Southwell and

Hall,⁷ and Abu-Safia *et al.*¹⁴ predict that sidelobes can be suppressed and spectral response of the filter can be improved through the use of matching layers and apodization functions. Apodization functions apply an envelope onto the sinusoidal rugate index profile, and matching layers provide an efficient transition between two optically different media, reducing Fresnel surface reflectance. Rugate filters were previously fabricated by continuously varying current density during anodic etching of crystalline silicon,^{8,15,16} and by continuously varying oxide/nitride content during chemical vapor deposition of silicon and aluminum oxynitrides.^{2,17,18} Pseudo-rugate filters, with thin discrete layers of constant index approximating the sinusoidal profile have also been achieved with techniques based on co-deposition.¹⁹ Experimental demonstration of apodization¹³ and continuous index matching to ambient⁷ design principles has proved challenging due to the difficulty in fabricating inhomogeneous thin film interference coatings while maintaining precise control of the film's optical response over a wide refractive index range.^{2,8}

Introducing nanometer-scale porosity in conventional optical materials modulates the dielectric response as described by effective-medium theory. The effective response is approximately the density-weighted sum of the bulk material and ambient responses. Varying the porosity of bulk Silicon ($n \sim$

The authors are with the Department of Physics, Queen's University, Kingston, Ontario K7L 3N6, Canada.

Received 2 December 2002; revised manuscript received 4 April 2003.

0003-6935/03/204212-08\$15.00/0

© 2003 Optical Society of America

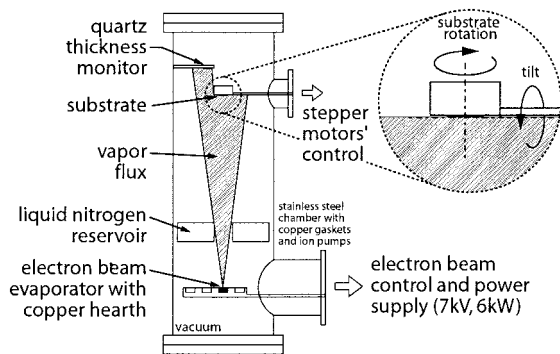


Fig. 1. Schematic of the GLAD system.

3.5) between 0 and 1 produces a variation of index between 3.5 and 1. Here the porosity of vacuum evaporated silicon thin films is varied dynamically with computer-controlled substrate motion during deposition onto substrates tilted with respect to the arriving vapor flux.

Glancing angle deposition (GLAD),^{20–22} an extension of earlier work on inclined substrate deposition^{23–26} is a reasonably simple technique for fabricating graded index optical coatings with a smoothly varying index.²¹ This paper demonstrates how GLAD was used in conjunction with a careful optical calibration and computer control of deposition geometry to fabricate complex apodized and matched rugate filters according to design specifications. Silicon was chosen as the optical material for the rugate filters because of its transparency in the optical communication wavelength band near 1.5 μm , its high refractive index, which enables a wide index spectrum and thus a range of bandwidth choices, and compatibility with integrated electronic or photonic structures. Many other evaporable materials could be used instead of silicon to suit particular optical-response requirements. As expected for room-temperature evaporated silicon, x-ray diffraction revealed highly amorphous silicon in all rugate films.

2. Glancing Angle Deposition

Figure 1 shows an outline of our deposition system, a copper-gasketed stainless-steel vacuum chamber with a 6 kW electron beam evaporator. The substrate is situated on a manipulator 50 cm directly above a 25-mm-diameter crucible, in a water-cooled hearth, where the silicon is melted and evaporated with a 7 kV electron beam. A dry scroll pump, a loadlock tubomolecular pump, and two large ion pumps evacuate the evaporation chamber and a cluster-tool-type sample distribution chamber. The deposition stage motion is managed with two computer-controlled stepper motors that tilt and rotate the substrate about a eucentric point in the center of the substrate surface. A liquid nitrogen reservoir is kept filled throughout the deposition to provide chamber cooling and to counter background-pressure rise from outgassing. The reservoir is designed as an annulus to allow deposition onto the

substrate and crystal-thickness monitor, yet to prevent deposition on the rest of the chamber. Throughout each filter deposition, the chamber pressure was maintained at $(1.3 \pm 0.7) \times 10^{-7}$ Pa, (1×10^{-9} Torr). After a stable evaporation rate is achieved, a LabVIEW-based computer control system takes control of the deposition process. The LabVIEW system controls the motion of two precise stepper motors that adjust the position of the substrate according to a calculated description of the desired position as a function of film thickness. The film thickness and deposition rate are measured throughout with a crystal-oscillator monitor, and the information is passed to the LabVIEW control system. The control system uses this feedback to adjust substrate motion for varying deposition rates. The deposition rate was approximately 0.5 nm/s, and the substrate temperature was (30 ± 3) °C as measured by a thermocouple gauge in the deposition stage. Deposition time was typically 1 hour for each of the 1.5- μm -thick rugate filters described.

Refractive index variation is accomplished by continuously varying film porosity.²¹ Nonlocal shadowing effects, where previously deposited film material prevents subsequent deposition in its geometric shadow, are greatly enhanced as the vapor incidence approaches a glancing angle. Limited surface mobility of adatoms prevents film growth in shadowed regions, and an atomic-scale dendritic structure evolves, consistent with other diffusion-limited aggregation processes.^{23,26} The film porosity is a strong function of the angle of arrival of the vapor flux onto the substrate with porosity increasing with tilt. If a substrate is tilted at a fixed angle relative to the vapor flux, and held motionless during deposition, the film grows inclined toward the source (at a growth angle smaller than the incidence angle),²² producing an optically bi-axial, birefringent medium.²⁷ When continuous, rapid substrate rotation is combined with vapor deposition at a large tilt angle ($>70^\circ$), the resulting microstructure is pillar-like, extending perpendicular to the substrate.²⁸ This rotation effectively eliminates in-plane anisotropy, and produces an optically uniaxial medium with the principal axis normal to the substrate surface. The refractive index along the normal axis is typically larger than the index in-plane ($n_{\text{inplane}} = 1.97$, $n_{\text{normal}} = 2.28$ for Si at 70° tilt, measured at 1000 nm). While the rugate filters described here were made with rapid substrate rotation (0.5 revolution/s) to eliminate in-plane birefringence effects, polarization-sensitive rugate filters are also possible with similar techniques.²⁹ The resulting physical microstructure is much smaller than the wavelengths of visible and infrared light so the incident radiation experiences a locally homogeneous material that produces little diffuse scatter, though this is a topic of continuing study. Arbitrary one-dimensional refractive index profiles can be achieved by varying the substrate tilt relative to the vapor; by controlling the film porosity, and therefore the refractive index, as a function of deposition time and film thickness.

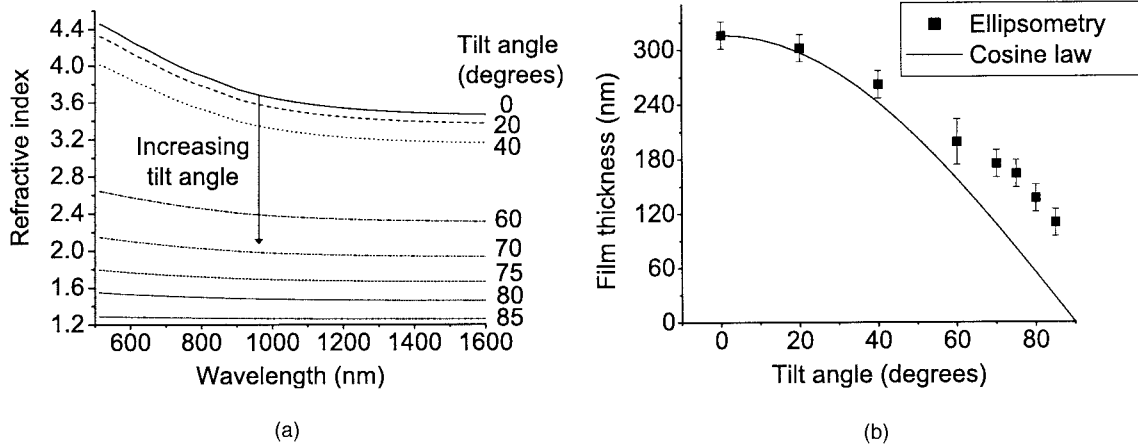


Fig. 2. Results of spectroscopic ellipsometry calibration. The set of films used for the study consisted of eight porous, amorphous silicon films made at constant substrate tilt angles. A Bruggemann uniaxial effective medium approximation model was used to extract index and thickness information. (a) Variation of refractive index with wavelength (for eight substrate tilt angles). The refractive index of the films decreases with the increasing substrate tilt as the films become more porous. (b) Variation of film thickness with substrate tilt angle. Increased atomic shadowing at higher deposition angles produces porosity that increases the thickness of the films above the cosine trend at all tilt angles.

3. Spectroscopic Ellipsometry Calibration

Calibration of the optical response of the films as a function of deposition conditions was performed with spectroscopic ellipsometry. Ellipsometry allows accurate measurement of refractive index, film thickness, and absorption, when used with an appropriate effective medium model. A Woollam M-2000, fixed angle, spectroscopic ellipsometer with a spectral range 370–1700 nm was used to determine simultaneously the real and imaginary parts of the dielectric function and the thickness of the calibration films. The set of calibration films consisted of eight porous silicon films deposited onto rotating substrates at constant deposition angles of 0°, 20°, 40°, 60°, 70°, 75°, 80°, and 85° (measured from the substrate normal), each film being nominally 200 nm thick as measured during growth with a quartz-oscillation thickness monitor. The ellipsometer was used to measure the Ψ and Δ parameters, defined by³⁰

$$\tan(\Psi)e^{i\Delta} = \frac{R_p}{R_s}, \quad (1)$$

where R_p/R_s is the complex ratio of the Fresnel reflection coefficients for p - and s - polarized light, respectively. This optical response was analyzed with effective medium software included with the Woollam ellipsometer, and based on a Bruggemann model.³¹ Owing to the columnar structure of the films, the dielectric response parallel to the columns is different than perpendicular, requiring anisotropic treatment in optical modeling. The optical axis (larger refractive index) of the films is along the direction of the columns (perpendicular to the surface) while the index is constant in all in-plane directions, arising from the symmetry of growth onto the rapidly rotating substrate. A Bruggemann uniaxial effective medium approximation (EMA) model was used and fit to measured response to extract index and

thickness information. The model consisted of two EMA constituents representing the optical response in the in-plane and perpendicular directions, with amorphous silicon, silicon dioxide, and air voids as components.³² The Levenberg–Marquardt regression algorithm was used to obtain parameters that minimize the difference between the experimental and model data. Because the silicon dioxide and air void constituents of the EMA have little spectral structure, the constituents are strongly correlated and not independently determinable. However, the correct dielectric values are measured with ellipsometry regardless of the details of the EMA. Figures 2(a) and 2(b) show the results of the calibration study. As expected, the refractive index of the films decreases with increasing deposition angles as the films become more porous, with the index approaching 1.0 (that of the air ambient) as tilt increases toward 90 deg. The physical thickness of the films (for a nominal thickness of 200 nm) also decreases with the increasing deposition angle, as expected, since the substrate sees a smaller effective area of the source at higher angles, with the rate per substrate area decreasing as a cosine of the tilt angle. The thickness, however, decreases less than a simple cosine because of the porosity produced by the increased atomic shadowing at higher deposition angles. Film thickness remains above the cosine trend at all tilt angles. Thickness values determined by ellipsometry were confirmed with scanning electron microscopy.

To design the optical response of the rugate filters, we assumed that the optical response of a thin layer within the rugate structure was equal to the response measured in the nominal 200-nm-thick calibration films. The layers are assumed to be thin enough to accurately approximate a smoothly varying optical response, as there are no discrete interfaces in the rugate films. This assumption also implies that we are expecting resonance scattering from the smooth

periodic features to be the mechanism responsible for the formation of the stop band. Nucleation and growth scaling effects³³ are expected to violate this assumption to some extent, but a comparison with fabricated films shows these effects to be minimal.

4. Apodized Filters

The refractive index profile of a simple rugate filter is usually expressed as²¹

$$n(x) = n_{\text{average}} + \frac{1}{2} n_{\text{peak}} \sin\left(\frac{4\pi n_{\text{average}} x}{\lambda_o}\right), \quad (2)$$

where n_{average} is the average index, n_{peak} is the peak-to-peak refractive index variation, x is the film thickness, and λ_o is the central wavelength of the filter. The results of the ellipsometry calibration study provided empirical information about the variation of refractive index n and film thickness x with the deposition angle. This calibration was used to calculate the desired orientation of the substrate relative to the vapor flux as a function of film thickness, to obtain the desired rugate refractive index profile.

A simple rugate, designed to show both the central stop band and the long-wavelength passband, is centered at $\lambda_o = 850$ nm, with $n_{\text{average}} = 1.72$, and $n_{\text{peak}} = 0.95$ with six periods of index oscillation. These parameters correspond to varying the substrate tilt angle between 63° and 86° with the total thickness of the film equal to 1500 nm. The film was deposited onto a Corning 7059, flat, glass substrate with an index of 1.52 at 850 nm. The index profile is shown in Fig. 3(a) and the corresponding calculated transmission spectrum is shown in Fig. 4(a) (simple). The decreased transmittance at short wavelengths is due to band-edge absorption in the silicon film.³² The calculated design spectra in Fig. 4(a) include an absorption model to allow direct comparison to measured results. These filters could be manufactured at higher central wavelengths (1.3–1.55 μm) with Si to avoid this absorption region, or other materials could be made nano-porous with this technique.

To explore the capabilities of this technique, more complex filters, incorporating envelope apodization functions and index matching layers, were designed, fabricated, and characterized. Keeping the number of index cycles constant at six, the effect of these designs on passband sidelobe suppression was compared.

The first variation from a simple rugate is a Gaussian apodization function imposed from the top and the bottom of the index profile, as shown in Fig. 3(b). The Gaussian was cut off at the profile edges at $1/e^2$ of the peak index amplitude. Next, Gaussian apodization was imposed only from the top of the refractive index profile as shown in Fig. 3(c). Figure 4(a) shows the silicon rugate filter transmission spectra calculated for the simple and apodized refractive index profiles. These theoretical transmission spectra were calculated using a MATLAB program based on the characteristic matrix method.³⁴ In the characteristic matrix method calculation each cycle of the refrac-

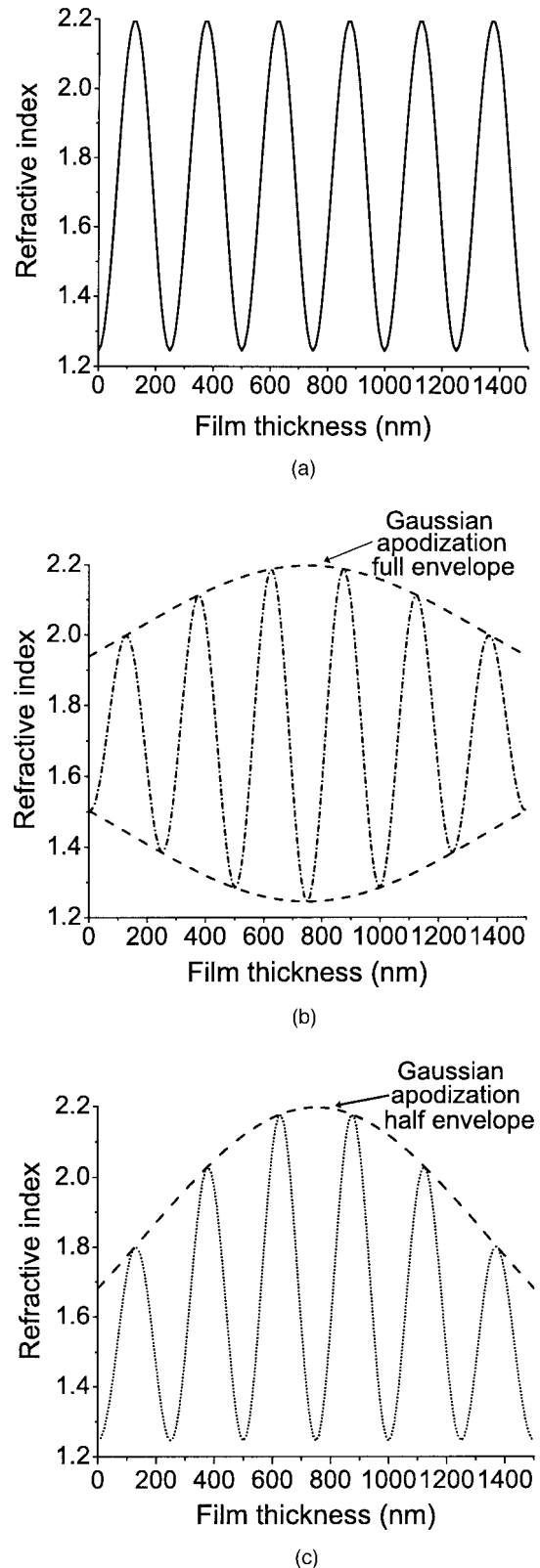


Fig. 3. Refractive index profiles for the rugate filter designs. (a) Simple rugate filter design with $\lambda_o = 850$ nm, $n_{\text{average}} = 1.72$, and $n_{\text{peak}} = 0.95$. (b) Fully-apodized rugate filter design. A Gaussian apodization function was imposed to the top and the bottom of the simple rugate index profile. (c) Half-apodized rugate filter design. A Gaussian apodization function was imposed to only the top of the simple rugate index profile.

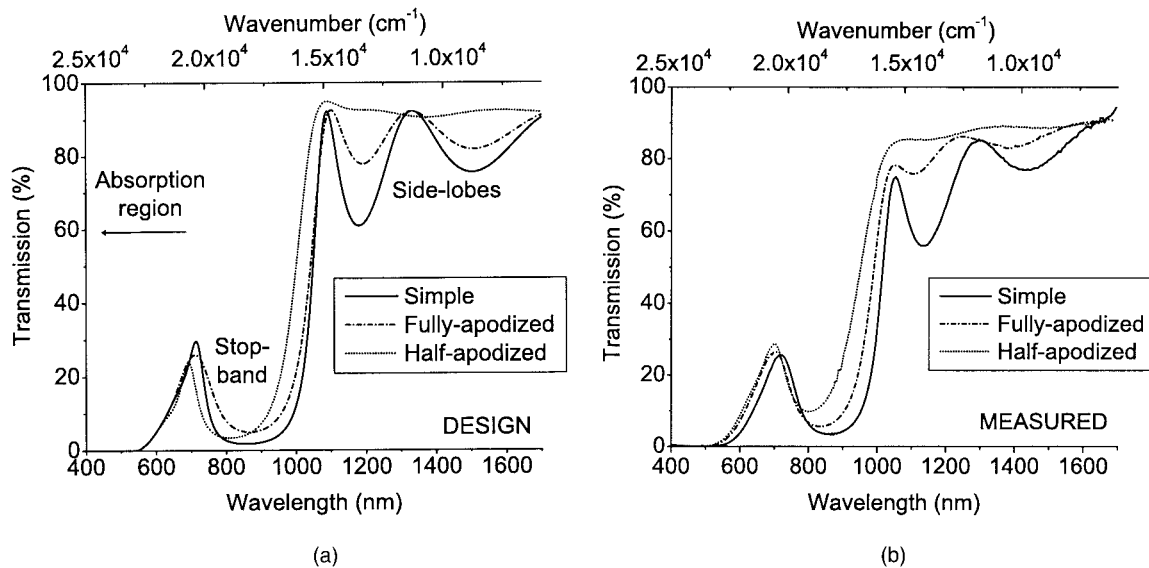


Fig. 4. Transmission spectra for the refractive index profiles shown in Fig. 3. (a) Theoretical transmission calculated using the characteristic matrix method. An absorption model was included in the calculation. (b) Measured transmission for the rugate filters grown with GLAD. The sidelobes are significantly reduced with apodization.

tive index profile was divided into 25 layers. Doubling the number of layers had negligible effect on the calculated transmission spectrum.

The calculated simple rugate spectrum in Fig. 4(a) (simple) clearly shows the stop band of the filter centered at approximately 850 nm, as well as the undesirable sidelobes. An ideal rugate filter would have 100% transmission for all wavelengths outside the stop band; a good filter should eliminate or at least greatly reduce the sidelobes. The expected improvement in filter spectral response with the addition of apodization functions is also seen in Fig. 4(a) (fully apodized and half apodized). Additional rugate periods increase stop-band reflectance. Filter thickness in this study was limited by the volume of the silicon source crucible; experimental demonstration of thicker filters will need to be performed with a large-source or continuous-feed industrial evaporator.

Figure 4(b) shows the transmission spectra measured through the fabricated rugate filters by using the ellipsometer in absolute transmission intensity mode. The spectral response of the fabricated filters is in good agreement with the designs, and the apodized filters indeed show significant sidelobe suppression around the stop bands. As predicted by theory,^{13,14} a full apodization increases transmittance in the passbands, and a half apodization essentially eliminates side-lobe oscillations.

5. Nanostructure

The morphological structure of manufactured rugate filters was analyzed with a Hitachi S-5200 field-emission scanning electron microscope (SEM). A cleaved edge of a simple rugate filter is shown in Fig. 5(a). Six distinct periods of the rugate profile are clearly distinguishable, and the porosity varies peri-

odically from the substrate (left) to the film surface (right). The thickness of the film is 1.5 μm , in agreement with design. Figure 5(b) is a scanning electron micrograph of the half-apodized rugate filter. Again, the six periods are clearly visible with the middle two periods and are distinctly denser than the outer periods, producing the larger index variation in the middle of this apodized design.

While the ellipsometry calibration and matrix method design procedure predicts filter response reasonably accurately, the apodized filters exhibit slightly smaller bandwidths, and reduced transmittance at longer wavelengths than theory predicts. The high-resolution SEM image of the rugate filter shown in Fig. 5(c) suggests these differences arise through complex microstructure effects in the evolving film. Periodically varying the tilt angle produces a type of perturbed ballistic aggregation, where the columns do not vary smoothly in thickness, but rather with many branches and protrusions with dimensions as small as 10 nm across (approximately 50 atoms). Stochastic arrival of vapor atoms, amplified by long-range atomic shadowing at high tilt angles, produces this branching structure that begins at atomic dimensions. The structure is self-affine, exhibiting similar morphological structures at varying length scales.³³ A more complete theoretical description of the optical response of these filters would require a treatment of coherent scattering from the morphological structure on all scales. The success of our simple calibration and one-dimensional Bragg resonance scattering model demonstrates that there is little coherent scattering from the fractal microstructure at the infrared wavelengths tested. Coherent scattering of light with a wavelength closer to the length scale of the nanostructure is predicted to produce higher-dimensional photonic crystal effects,

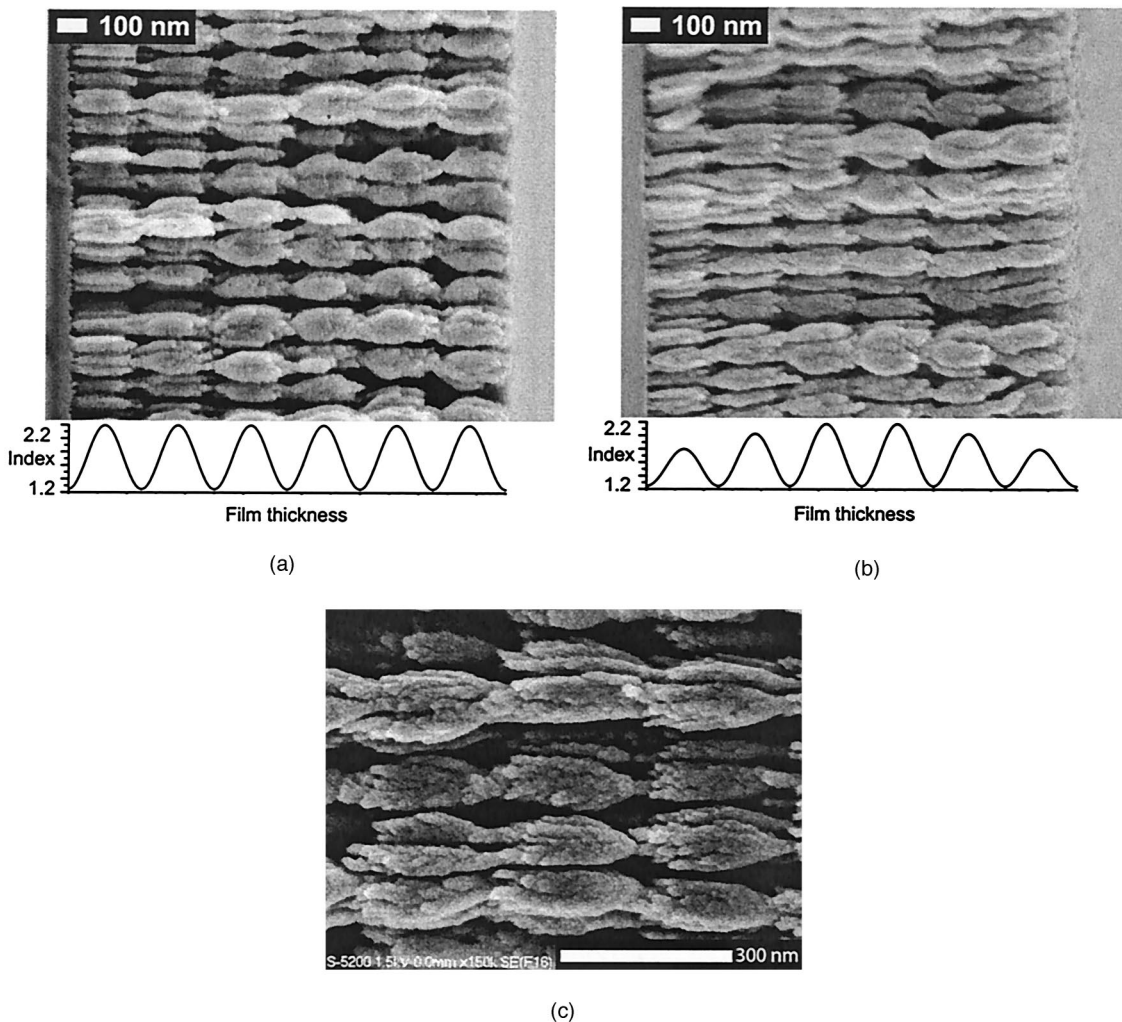


Fig. 5. Nanostructure of the rugate filters studied with SEM. (a) Simple rugate filter. (b) Half-apodized rugate filter. (c) High resolution SEM image of the simple rugate filter showing perturbed ballistic aggregation. Branching structure is resolved to the resolution limit of the microscope (approximately 10 nm).

such as anomalous dispersion and photonic bandgaps.^{35,36} Growth complexity and ordering phenomenon are currently being investigated with three-dimensional Monte Carlo modeling and will be accommodated in filter design when microstructure evolution effects are more fully understood.

6. Matched Rugate Filters

A critical optical component, an index-matching or antireflection layer, can be fabricated in a novel way with GLAD. Continuously grading the refractive index to match the ambient index produces a wideband antireflection response. A simple, one layer antireflection coating³⁴ whose index is the mean of the average rugate index and that of air $n = (n_{\text{average}} \times n_{\text{air}})^{1/2}$, and that has a quarter-wave thickness at the central wavelength of the filter [Fig. 6(a)] suppresses the sidelobes near the stop band as shown in Fig. 7 (quarter-wave matching). However, the quarter-wave matching layer reduces the sidelobes only near the central wavelength. Southwell⁷ has shown that a quintic index matching region, which smoothly

matches the adjacent media, produces more wide-band suppression. A quintic is a fifth-order polynomial between the substrate and the average rugate index with the first and second derivatives equal to zero at the interfaces. The refractive-index profile is defined by

$$n(x) = n_{\text{air}} + (n_{\text{average}} - n_{\text{air}}) \left[10 \left(\frac{x}{t} \right)^3 - 15 \left(\frac{x}{t} \right)^4 + 6 \left(\frac{x}{t} \right)^5 \right], \quad (3)$$

where n_{average} is the average rugate index, n_{air} is the refractive index of the surrounding air, x is film thickness, and t is the total thickness of the matching layer. The thickness of the matching layer t determines the width of the wavelength region over which antireflection occurs. A significant advantage of our technique is that wide index variation is possible, as the index may be varied from that of the bulk material to that of the ambient, therefore matching to air

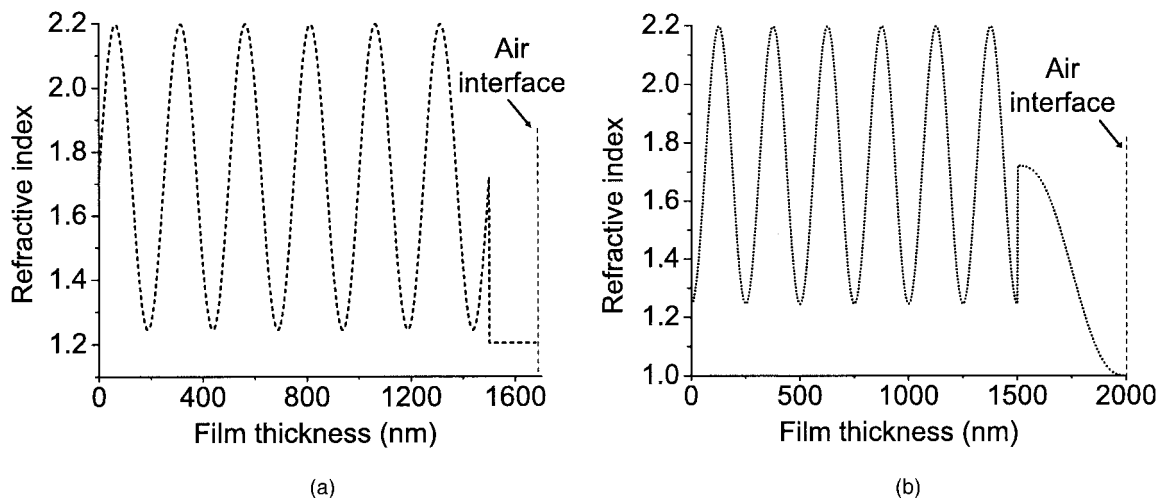


Fig. 6. Effect of matching layers on the transmission spectrum of the simple rugate filter. (a) Refractive index profile for the simple rugate filter with a quarter-wave matching layer to air. (b) Refractive index profile for the simple rugate filter with a quintic matching layer to air. This design provides smooth index matching down to the refractive index of air, which is a novel result.

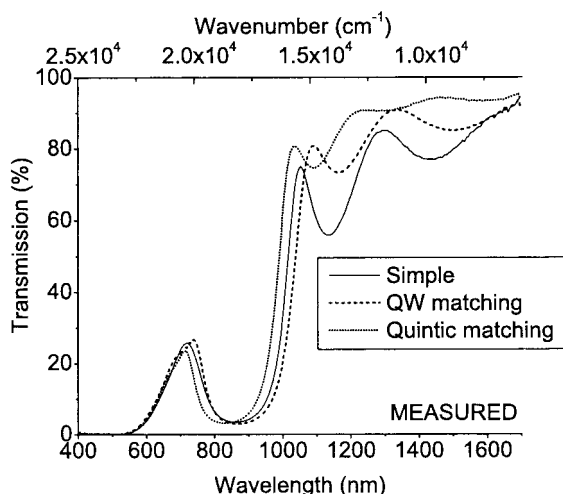


Fig. 7. Transmission spectra for the refractive index profiles shown in Fig. 6. The quarter-wave design reduces the sidelobes near the central wavelength, whereas quintic matching produces a wideband suppression.

of index $n_{\text{air}} = 1$ is possible. Figure 6(b) shows the refractive-index profile of the rugate with the quintic matching to air, and Fig. 7 (quintic matching) shows the corresponding measured transmission spectrum. As predicted by theory,⁷ the quintic matching layer essentially eliminates reflection in the passband over a broad wavelength region.

7. Conclusions

Interference filters fabricated from vacuum evaporated silicon, with controlled porosity achieved with glancing angle deposition, are shown to be versatile photonic devices with designable response characteristics. The high porosity of the film materials is interesting both as an engineering stability problem and as an opportunity for dynamic control of an optical response, or for sensing of fluids or gases.

Liquid-crystal infiltration into the film voids will likely enable electro-optic control of the band-edge position and amplitude, and fluid or gas infiltration¹⁵ will shift the optical response in an observable way. As the growth technique employs vacuum deposition, it offers benefits over etched porous silicon and etched porous silicon rugates through improved device integration suitability, wide refractive-index variation (including continuously to near ambient), widely variable pore dimensions, and opportunities through material variation.

Oxidation of the film has not yet been rigorously studied, but a qualitative sampling suggests rapid surface oxidation upon removal from a vacuum, followed by a long optically stable lifetime (the band edge of a simple rugate shifted less than 5 nm over one year of room temperature storage with varying humidity).

Structural ordering of the silicon material in the plane of the substrate will produce resonant scattering or photonic crystal effects if the order is sufficiently regular, and if the probing light wavelength matches the structural periodicity. Physical characterization of the silicon rugate structure with scanning electron microscopy reveals an in-plane inhomogeneity with some appearance of periodic structure. The period of the structure scales from near atomic dimensions to some hundreds of nanometers. While it appears that the structure lacks significant long-range order, resonant scattering from these or more regularly ordered evaporated film structures are predicted to yield photonic band gaps and anomalous dispersion properties with applications in optical computation and communication.^{35,36}

The novel quintic antireflection (or index-matching) coating is an important contribution to the optical engineering toolbox, enabling near-lossless coupling between optical media with considerably different indexes of refraction. Employing a liquid or polymer index-matching fluid within the voids of the

film may allow improved coupling between optical components, possibly while simultaneously joining components and stabilizing the porous film structure. Diffuse scattering from the microstructure will need to be further characterized to determine the applicability of these antireflection coatings in communications or high-power laser applications. Finally, mechanical stability issues must be addressed through performance versus stability optimization, and intelligent integration and packaging. Industrial scaleup of the glancing angle deposition process has yet to be achieved, but appears possible with appropriate process and equipment design.

This work was supported by the Canadian Institute for Photonic Innovations (CIPI), the Natural Sciences and Engineering Research Council of Canada (NSERC), and the Canada Research Chairs program.

References

1. A. Macleod, "Challenges in the design and production of narrow band filters for optical fiber telecommunications," in *Optical and Infrared Thin Films*, M. L. Fulton, ed., Proc. SPIE **4094**, 46–57 (2000).
2. L. Martinu and D. Poitras, "Plasma deposition of optical films and coatings: A review," *J. Vac. Sci. & Technol. A* **18**, 2619–2645 (2000).
3. D. A. Linkens, M. F. Abbod, J. Metcalfe, and B. Nichols, "Modeling and fabrication of optical interference rugate filters," *ISA Transactions* **40**, 2–16 (2001).
4. B. G. Bovard, "Rugate filter theory: an overview," *Appl. Opt.* **32**, 5427–5442 (1993).
5. H. Fabricius, "Gradient-index filters: designing filters with steep skirts, high reflection, and quintic matching layers," *Appl. Opt.* **31**, 5191–5196 (1992).
6. R. R. Willey, "Rugate broadband antireflection coating design," in *Current Developments in Optical Engineering and Commercial Optics*, R. E. Fischer, H. M. Pollicove, and W. J. Smith, eds., Proc. SPIE **1168**, 224–228 (1989).
7. W. H. Southwell and R. L. Hall, "Rugate filter sidelobe suppression using quintic and rugated quintic matching layers," *Appl. Opt.* **28**, 2949–2951 (1989).
8. M. G. Berger, M. Arens-Fischer, M. Tonissen, M. Kruger, S. Billat, H. Luth, S. Hilbrich, W. Thieb, and P. Grosse, "Dielectric filters made of PS: advanced performance by oxidation and new layer structures," *Thin Solid Films* **297**, 237–240 (1997).
9. S. Lim, S. Shih, and J. G. Wager, "Design and fabrication of a double bandstop rugate filter grown by plasma-enhanced chemical vapor deposition," *Thin Solid Films* **277**, 144–146 (1996).
10. S. Cianci, J. Bland-Hawthorn, and J. O'Byrne, "Rugate filters: quasars beyond $z \sim 7?$," *Astron. Soc. Pac. Conf. Ser.* **195**, 391–397 (2000).
11. J. N. Winn, Y. Fink, S. Fan, and J. D. Joannopoulos, "Omnidirectional reflection from a one-dimensional photonic crystal," *Opt. Lett.* **23**, 1573–1575 (1998).
12. W. H. Southwell, "Spectral response calculations of rugate filters using coupled-wave theory," *J. Opt. Soc. Am. A* **5**, 1558–1564 (1988).
13. W. H. Southwell, "Using apodization functions to reduce sidelobes in rugate filters," *Appl. Opt.* **28**, 5091–5094 (1989).
14. H. A. Abu-Safia, A. I. Al-Sharif, and I. O. Aljarayesh, "Rugate filter sidelobe suppression using half-apodization," *Appl. Opt.* **32**, 4831–4835 (1993).
15. P. A. Snow, E. K. Squire, P. St. J. Russell, and L. T. Canham, "Vapor sensing using the optical properties of porous silicon Bragg mirrors," *J. Appl. Phys.* **86**, 1781–1784 (1999).
16. F. Cunin, T. A. Schmedake, J. R. Link, Y. Y. Li, J. Koh, S. N. Bhatia, and M. J. Sailor, "Biomolecular screening with encoded porous-silicon photonic crystals," *Nature Materials* **1**, 39–41 (2002).
17. G. Placido, J. Russell, and Z. Gou, "Graded-index films using aluminium oxynitrides," in *Developments in Optical Coating Coatings*, I. Reid, ed., Proc. SPIE **2776**, 159–168 (1996).
18. S. Lim, J. H. Ryu, J. F. Wager, and T. K. Plant, "Rugate filters grown by plasma-enhanced chemical vapor deposition," *Thin Solid Films* **245**, (1994).
19. R. Overend, D. R. Gibson, and R. Marshall, "Rugate filter fabrication using neutral cluster beam deposition," *Vacuum* **43**, 51–54 (1992).
20. K. Robbie, M. J. Brett, and A. Lakhtakia, "Chiral sculpted thin films," *Nature* **384**, 616–616 (1996).
21. K. Robbie, A. J. P. Hnatiw, M. J. Brett, R. I. MacDonald, and N. J. McMullin, "Inhomogeneous thin film optical filters fabricated using glancing angle deposition," *Electron. Lett.* **33**, 1213–1214 (1997).
22. K. Robbie and M. J. Brett, "Sculptured thin films and glancing angle deposition: Growth mechanics and applications," *J. Vac. Sci. Technol. A* **15**, 1460–1465 (1997).
23. R. Messier, V. C. Venugopal, and P. D. Sunal, "Origin and evolution of sculptured thin films," *J. Vac. Sci. Technol. A* **18**, 1538–1545 (2000).
24. T. Motohiro and Y. Taga, "Thin film retardation plate by oblique deposition," *Appl. Opt.* **28**, 2466–2482 (1989).
25. I. J. Hodgkinson, F. Horowitz, H. A. Macleod, M. Sikkens, and J. J. Wharton, "Measurement of the principal refractive indices of thin films deposited at oblique incidence," *J. Opt. Soc. Am. A* **2**, 1693–1697 (1985).
26. L. Abelmann and C. Lodder, "Oblique evaporation and surface diffusion," *Thin Solid Films* **305**, 1–21 (1997).
27. I. J. Hodgkinson and Q. Hong Wu, *Birefringent Thin Films and Polarizing Elements* (World Scientific, Singapore, 1997).
28. K. Robbie, C. Shafail, and M. J. Brett, "Thin films with nanometer-scale pillar microstructure," *J. Mater. Res.* **14**, 3158–3163 (1999).
29. A. J. McPhun, Q. H. Wu, and I. J. Hodgkinson, "Birefringent rugate filters," *Electron. Lett.* **34**, 360–361 (1998).
30. H. G. Tompkins and W. A. McGahan, *Spectroscopic Ellipsometry and Reflectometry* (Wiley, New York, 1999).
31. S. Zangoie, M. Schubert, C. Trimble, D. W. Thompson, and J. A. Woollam, "Infrared ellipsometry characterization of porous silicon Bragg reflectors," *Appl. Opt.* **40**, 906–912 (2001).
32. E. D. Palik, *Handbook of Optical Constants of Solids* (Academic, San Diego, Calif., 1985).
33. A. L. Barabasi and H. E. Stanley, *Fractal Concepts in Surface Growth* (Cambridge University, Cambridge, UK, 1995).
34. A. Thelen, *Design of Optical Interference Coatings* (McGraw-Hill Optical and Electro-Optical Engineering Series, McGraw-Hill, New York, 1989).
35. O. Toader and S. John, "Square spiral photonic crystals: Robust architecture for microfabrication of materials with large three-dimensional photonic band gaps," *Phys. Rev. E* **66**, 1–18 (2002).
36. O. Toader and S. John, "Proposed square spiral microfabrication architecture for large three-dimensional photonic band gap crystals," *Science* **292**, 1133–1135 (2001).